International Journal of Computational and Experimental Science and ENgineering (IJCESEN)

Vol. 11-No.4 (2025) pp. 7391-7404
http://www.ijcesen.com

ISSN: 2149-9144

Research Article

Exploring the Potential of Vacancy-Ordered Cs_2PtI_6 Perovskite as a Lead-Free Absorber for Next-Generation Solar Cells via Modeling and Simulation

Hayat Arbouz*

Univerity Saad Dahlab Blida 1, Faculty of Sciences, Physics Department, 09000, Blida-Algeria
* **Corresponding Author Email:** arbouz_hayat@univ-blida.dz - **ORCID:** 0000-0003-2780-5215

Article Info:

DOI: 10.22399/ijcesen.3281
Received : 10 May 2025
Accepted : 20 September 2025

Keywords

Photovoltaics
Solar Cell
Perovskite
Simulation
Lead-Free

Abstract:

This study explores the potential of the vacancy-ordered perovskite material Cs_2PtI_6, which is inorganic and lead-free, as an absorber layer in a single-junction solar cell. The research is based on modeling, simulation, and subsequent optimization of the cell structure to achieve optimal conversion efficiency. A baseline structure FTO/TiO_2/Cs_2PtI_6/Spiro-OMeTAD/Au was designed as the starting point for simulations. The effects of various physical factors on key photovoltaic parameters were evaluated, including the thicknesses of the absorber, electron transport layer (ETL), and hole transport layer (HTL), as well as the defect density within the Cs_2PtI_6 material and at its interfaces with the ETL and HTL. For this purpose, a mathematical model was established to investigate the combined effects of parameters, supported by contour plot analysis. Moreover, alternative materials for the ETL and HTL, featuring different physical properties and band alignments compared to those in the baseline structure, were investigated. The study also examined how the height of the energy barrier at the rear interface between the HTL and the metal layer influences device performance. Based on these findings, an optimized structure FTO/CeO_2/Cs_2PtI_6/Cu_2O/Carbon was developed. This configuration achieved a conversion efficiency of 18.54%, demonstrating its superiority over the baseline design and other comparable solar cell architectures. Overall, this work highlights the promising potential of vacancy-ordered Cs_2PtI_6 perovskite and contributes to the advancement of next-generation solar cell technologies.

1. Introduction

Research in renewable energy is rapidly expanding to meet the growing and increasingly urgent demand for sustainable solutions. Among the various technologies, electricity generation from photovoltaic solar sources stands out as a leading contender, showcasing significant potential for the future [1]. While silicon-based technologies have historically dominated this landscape due to their proven efficiency, the rise of perovskite technologies offers an exciting new direction for advancements in renewable energy production [2]. The growing interest in perovskites is driven by their rapid development and remarkable records in conversion efficiency, coupled with cost-effective manufacturing technique [3].

Perovskites are a category of materials distinguished by a unique crystal structure, typically described by the formula ABX_3. The name "perovskite" derives from the mineral calcium titanium oxide ($CaTiO_3$), which was first discovered in 1839 [4]. Over the years, this classification has broadened to include a diverse range of compounds that exhibit remarkable properties such as ferroelectricity, superconductivity, and magnetoreistance [5]. However, the advancement of perovskites has been significantly influenced by their potential for solar energy applications. Although organic-inorganic hybrid perovskites have demonstrated high efficiencies, research efforts are increasingly concentrating on the development of inorganic and lead-free perovskites [6]. This transition is largely driven by environmental and health concerns related to the use of lead in conventional perovskite materials [7], in addition to stability issues due to the volatility of the organic components [8]. All-inorganic perovskites, such as those based on cesium (Cs), show significantly improved thermal and moisture stability, making them more appropriate for long-term deployment in photovoltaic devices [9]. Several studies have

focused on the development of photovoltaic structures based on inorganic perovskites containing cesium [10-11]. Vacancy-ordered perovskites, including materials like Cs_2PtI_6 and Cs_2TeI_6 show considerable promise for solar cell applications due to their distinctive structural and electronic characteristics [12]. They can be tailored to have band gaps within the optimal range of 0.9–1.6 eV, facilitating theoretical efficiencies that exceed 25%. Furthermore, vacancy-ordered perovskites are generally more stable and less toxic than conventional lead-based perovskites, making them more environmentally friendly options [13]. This research focuses on the modeling and optimization of a perovskite solar cell incorporating a fully metallic, lead-free perovskite absorber layer, specifically Cs_2PtI_6. An initial device architecture was established as the basis for simulation studies, comprising the following layers: fluorine-doped tin oxide (FTO), titanium dioxide (TiO_2), Cs_2PtI_6, spiro-OMeTAD, and gold (Au). The performance of the baseline solar cell was evaluated using a simulation model described in subsequent sections, generating benchmark data for comparative purposes. Following this, the impact of several physical parameters on device performance was investigated, alongside the selection of appropriate materials for the electron transport layer (ETL) and hole transport layer (HTL) through the evaluation of alternative candidates. The subsequent phase involves optimizing the identified parameters to develop an improved device architecture aimed at maximizing photovoltaic efficiency, with an emphasis on fully inorganic material systems. This study aims to explore the potential of the vacancy-ordered perovskite absorber Cs2PtI6 for use in solar cell structures and ultimately strives to promote the development of high-efficiency, lead-free perovskite solar cells, contributing significantly to the field of photovoltaics.

2. Material and Methods

2.1 Cs_2PtI_6 Material

Cs_2PtI_6 presents a compelling alternative to traditional perovskites due to its distinctive structural properties, environmental safety, and superior performance characteristics. With a narrow optical bandgap, Cs_2PtI_6 features a double perovskite structure, where cesium (Cs) occupies the A-sites, platinum (Pt) is situated at the B-site, and iodine (I) anions form octahedral coordination around the Pt atoms. It crystallizes in a cubic face-centered structure (space group $Fm\bar{3}m$) characterized by vacancy ordering in the B-site of the perovskite lattice [14]. This composition confers excellent chemical and environmental stability, including resistance to air, moisture, and extreme pH conditions. the heavy Pt atoms act as phonon rattlers, which strongly scatter lattice vibrations and result in ultralow lattice thermal conductivity (~0.15 W/mK), enhancing thermoelectric potential [15]. Despite the higher cost of Pt compared to lead, its excellent chemical stability, oxidation resistance, and ability to form a robust perovskite lattice make Cs_2PtI_6 a valuable model system for developing stable, non-toxic perovskite materials with promising optoelectronic and thermoelectric properties. Performed density functional theory (DFT) simulations to systematically explore the structural, electronic, and optical properties of mixed-halide perovskites $Cs_2PtI_{6-x}Br_x$, revealing a tunable bandgap ranging from 1.4 to 2.6 eV as bromide substitution increases [16]. Scharts etal [17], reported that synthesized high-purity Cs_2PtI_6 crystals via atmospheric solution processing employing CsI and PtI_4 precursors dissolved in a DMF:DMSO:GBL solvent system, resulting in well-defined lattice parameters near 8.3 Å. Assessed material stability by calculating the enthalpy of formation using the GGA-PBE functional; the observed negative enthalpy values confirm the thermodynamic stability robustness of Cs_2PtI_6 [18] . Characterization of charge transport properties confirmed high hole mobility indicating efficient charge extraction comparable to $MAPbI_3$, but with improved chemical stability [19]. UV-Vis-NIR spectroscopy combined with Tauc diagram analysis validates the direct bandgap nature (1.36 eV-1.4 eV) of Cs_2PtI_6 and quantifies the high absorption coefficients in the 350-450 nm spectra [20]. Analysis of the reflectivity and loss functions over the entire solar spectrum reveals low reflectivity and minimal energy loss, ideal for photovoltaic efficiency. These promising factors allow us to consider Cs_2PtI_6 as a promising absorber for photovoltaic applications.

2.2 Baseline Structure

This study aims to model and simulate the performance of Cs_2PtI_6 perovskite solar cell. To support this investigation, an ititial structure design was created as the starting point, including the following layers: FTO (Fluorine-doped Tin Oxide)/TiO_2/Cs_2PtI_6 / spiro-OMeTAD/Au (Gold) [21].

FTO is has been choosen as the transparent conductive oxide window layer material with an appropriate thickness of 300nm ,this material is highly transparent to allow the entrance of light and strongly n-type doped to ensure an optimal extraction and passage of the photogenerated electrons. TiO_2 is used as the n-type electron transport layer (ETL). This material has a high electron mobility to ensure the transport of electons

and at the same time contributes to minimize reflections and enhance the chance to photons reaching the absorbing layer. The organic p-type material Spiro-OMeTAD (2,2',7,7'-Tetrakis[N,N-di(4-methoxyphenyl)amino]-9,9'-spirobifluorene) serves as the hole transport layer (HTL) in the device structure. This layer possesses essential properties that facilitate the efficient transport of holes toward the back metallic contact, while also enhancing the interface between the perovskite absorber and the back electrode.

A: is a wavelength-independent constant, and E_g is the energy of the bandgap. h is the constant of Planck and c is the speed of light.

Three types of recombination were considered dominant in this study:

- Recombination due to the density of defects in the absorber.

Table 1. *Input parameters for materials used in the primary device*

Input parameters	**FTO [22]**	**ETL (TiO_2) [23]**	**Cs_2 Pt I_6 [24]**	**HTL(Spiro-OMeTAD) [25]**
Thickness, d [nm]	350	100	800	300
Band gap, E_g [eV]	3.50	3.26	1.37	2.20
Electron Affinity, χ [eV]	4.00	4.00	4.30	2.90
Permittivity, ε_r	9	10	4.8	3.00
Electron mobility, μ_n [$cm^2\ V^{-1}s^{-1}$]	20	100	62.6	0.02
Hole mobility, μ_p [$cm^2\ V^{-1}s^{-1}$]	10	25	62.6	0.0002
CB Effective density of states, N_C [cm^{-3}]	2.2×10^{18}	2.0×10^{17}	3.0×10^{14}	1.0×10^{21}
VB Effective density of states, N_V [cm^{-3}]	1.8×10^{19}	10×10^{17}	1.0×10^{17}	1.0×10^{21}
Density of n-type doping, N_D [cm^{-3}]	1.0×10^{19}	1.0×10^{18}	/	/
Density of p-type doping, N_A [cm^{-3}]	/	/	1.0×10^{15}	1.0×10^{18}
Defect Density N_t [cm^{-3}]	/	1.0×10^{15}	1.0×10^{15}	1.0×10^{15}

Table 2*. Cell interface Parameters* [26].

Parameters	**ETL**	**HTL**	**HTL/Absorber**	**Absorber/ETL**
Density of Defects, N_t [cm^{-3}]	10^{15}	10^{15}	10^{14}	10^{14}
Electron capture cross section, σ_n [cm^{-2}]	10^{-15}	10^{-15}	10^{-19}	10^{-19}
Hole capture cross section, σ_p [cm^{-2}]	10^{-15}	10^{-15}	10^{-18}	10^{-18}

The back terminal electrode is made of gold with a work function of 5.1 eV and a high electrical conductivity. The thickness of ETL, absorber and HTL layers have been set at 100nm, 800 nm and 100 nm in the primary structure, but optimized later to reach a higher efficiency, after the simulation work. A detailed description of the material properties of each layer is given in Table 1. Interfacial parameters at the front and rear interfaces are given in Table 2.

2.3 Computational Approach

In this work, several sub-models have been introduced into the simulation program for the purpose of calculating the current-voltage characteristic and extracting photovoltaic parameters.

The model of Tauc , is used to calculate the coefficient of absorption as a function of the wavelength λ .

$$\alpha(\lambda) = A.(\frac{hc}{\lambda} - E_g)^{1/2} \quad (1)$$

For this, the Schockley-Read-Hall model [21*27], expressed in equation 2.

$$R_{SRH} = \frac{n.p - n_i^2}{\tau_n.(n+n_i) + \tau_p.(p+n_i)} \quad (2)$$

n and p represent the concentrations of electrons and holes. τ_n and τ_p are carrier life-times. n_i is intrinsic density of charges.

Recombination at the interfaces between the absorber and the neighboring layers. The interface recombination velocity at the boundaries of the absorber is expressed as follows:

$$S_{n,p} = \sigma_{n,p,}.V_{th}.N_{tn,p} \quad (3)$$

$N_{tn,p}$ is the front/back interface density.V_{th} is the thermal velocity. $\sigma_{n,p}$ is the electron/hole capture cross section at interfaces.

- Recombination at the interface between HTL layer and rear metal contact.

The rear contact of the device may induce a schottky barrier. Therefore, the Schottky barrier Metal/HTL is evaluated as follows [27]:

$$\Phi_b = \varphi_m - (\chi_{HTL} - k.T.ln(\frac{N_{V,HTL}}{N_{a,HTL}})) \quad (4)$$

φ_m is the work function of the back metal contact, and χ_{HTL} is the electron affinity of the HTL material.

The photo generated current density is calculated by:

$$J_{ph} = q \int_{\lambda_{min}}^{\lambda_{max}} F(\lambda).EQE(\lambda)d\lambda \quad (5)$$

λ_{min} and λ_{max} are minimum and maximum wavelengths, q is the electron charge, $F(\lambda)$ is the solar spectrum and $EQE(\lambda)$ is the external quantum efficiency of the cell.

The equivalent circuit of the current-voltage characteristics is evaluated admiting a two-diode model [28].

$$J = J_{ph} - (J_0 + J_s + J_d).\left(e^{\frac{q.(V-JR_S)}{2kT}} - 1\right) - \frac{V-J.R_S}{R_{sh}} \quad (6)$$

J_0 : is the recombination reverse dark current density

J_s : is the interface recombination contribution in current density losses. This later depends on the conduction band offset (CBO) and valence band offset (VBO) at the boundaries of the absorber .

J_d : is the Schottky diode reverse saturation current density.

The key photovoltaic parameters were calculated using the expressions detailed in [29] This model was developed to calculate the characteristics current -voltage J-V and photovoltaic parameters and assess their dependence on key physical variables, such as layer thicknesses, recombination and bandgap energy mismatch between the layers. The purpose of the work is to propose an optimized structure that maximizes photovoltaic efficiency by optimizing the factors that alter performance.

3. Results and Discussions

3.1 Simultaneous Effect of the Absorber Thickness and Defect Density

The thickness of the perovskite layer plays a crucial role in determining the efficiency of solar cells. Studies indicate that an optimal thickness exists, which maximizes light absorption while minimizing recombination losses.

It has been demonstrated that a thickness of approximately 0.5 μm allows for sufficient generation of electron-hole pairs without compromising the electric field strength. However, increasing the thickness beyond this optimum can lead to diminished performance due to reduced electric fields and increased recombination rates.

Defect density within the perovskite layer is another vital factor affecting photovoltaic performance. High defect densities can introduce additional recombination centers, leading to reduced charge carrier lifetimes and lower overall efficiency [30]. The relationship between defect density and efficiency highlights the necessity for precise control over material quality during fabrication.

While thickness and defect density are often optimized independently, there is a compelling argument for their simultaneous variation. This approach allows for a more comprehensive understanding of how these parameters interact and influence the overall photovoltaic characteristics of perovskite materials. Studies have indicated that variations in both thickness and defect density can lead to nuanced changes in key performance metrics [31]. Contour plots are valuable tools for understanding the intricate relationship between absorber thickness and defect density in perovskite solar cells. By optimizing both parameters together, the performance of the device can be enhenced. To this end, Figure 1. presents a contour plot illustrating the power conversion efficiency as a function of thickness, ranging from 0.5 μm to 2 μm, and perovskite defect density, spanning from 10^{12} cm^{-3} to 10^{20} cm^{-3}. The contour plot indicates that lower defect densities (e.g., approximately 10^{12} cm^{-3}) are associated with higher PCE values, while higher defect densities result in a marked decline in efficiency. It is also highlited from the contour plot the areas where optimal thickness and low defect density coexist, lead to maximum PCE (e.g., thickness varying from 1μm to 2μm and N_t varying from 10^{14} cm^{-3} to 10^{16} cm^{-3}). The figure reveals an optimal thickness for Cs_2PtI_6 absorber around 1.5 μm, where power conversion efficiency (PCE) reaches its peak. At this thickness, the material effectively absorbs light while maintaining adequate electric field strength for efficient charge transport.

3.2 Simultaneous Effect of ETL and Cs_2PtI_6 Thicknesses

The electron transport layer (ETL) is essential for effective charge extraction from the perovskite layer. Its thickness influences the efficiency of electron extraction while minimizing recombination losses. However, the optimal thicknesses of the ETL vary depending on the material used. A proper alignment between the conduction band of the ETL and that of the perovskite is crucial for maximizing charge

collection efficiency. Reducing band offsets can lead to significantly improved device performance.Simultaneous optimization of both layers is vital, as the performance of one layer can have a considerable impact on the other. For instance, an optimal thickness of the perovskite may require a specific thickness of the ETL to maximize charge extraction without introducing excessive recombination losses. This approach to joint optimization can result in energy conversion efficiencies that surpass those achieved through independent optimizations. The simultaneous effect of varying the electron transport layer (ETL) and Cs_2PtI_6 thickness was investigated in this study. Several ETL materials with different properties and conduction band energy alignments with the

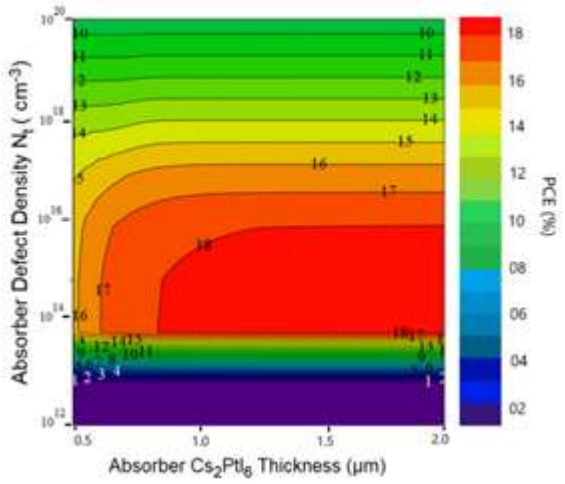

Figure 1. *Contour Plot of PCE of Cs_2PtI_6 solar cell as a function of absorber thickness and absorbr defect density.*

perovskite Cs_2PtI_6 absorber were analyzed through contour plot analysis of power conversion efficiency (PCE).The ETL thickness varied from 50 nm to 300 nm, while the CsPtI thickness ranged from 0.5 µm to 3.5 µm. Figure 2 shows the results obtained.All contour plots clearly indicate the zones of optimized thicknesses that lead to a peak in power conversion efficiency (PCE). While these zones vary from material to material, some electron transport layers (ETLs) exhibit similar behavior. For the TiO_2 ETL used in the primary structure, an efficiency of up to 18% is achieved only when the ETL thickness exceeds 120 nm and when using larger Cs_2PtI_6 absorbers greater than 2.6 µm. The structures based on SnO_2 and CeO_2 exhibit similar behavior, requiring only a very thin ETL thickness of 50 nm for large absorber greater than 2.6 µm for SnO_2 and 2.7 µm for CeO_2 to achieve an efficiency of 18.5%. For CdTe, the optimal ETL thickness must be between 230 nm and 250 nm when the absorber thickness exceeds 1.5 µm to achieve a yield of 17.5%. If the absorber thickness is reduced to between 900 nm and 1.5 µm, the ETL thickness must be greater than 250 nm to achieve a similar yield. Finally, a Cs_2PtI_6 absorber thickness of around 1.5 µm or more requires an organic C60 or PCBM ETL thickness of less than 100 nm to achieve a maximum efficiency of 18%. Through the analysis of these contour maps, we can identify the ideal thicknesses for the ETL and CsPtI layers corresponding to each ETL material. This enables us to pinpoint the configurations that achieve the maximum conversion efficiency. The results are shown in Table 3.Simulation results and contour map analysis indicate that the base structure, composed of a TiO_2 lectron transport layer (ETL) and a Cs_2PtI_6 perovskite layer, achieves a conversion efficiency of 18.48% with layer thicknesses of 150 nm and 2.5 µm, respectively. Interestingly, the same efficiency is attainable when CeO_2 is used as the ETL material, with reduced thicknesses of 50 nm for the ETL and 2.0 µm for the perovskite layer.

3.3 Optimization of the HTL Layer

The Hole Transport Layer (HTL) is a vital component in the structure of perovskite solar cells (PSCs) as it efficiently extracts holes from the perovskite absorber and transports them to the metal contact, thereby enhancing the overall efficiency of the solar cell. By facilitating smooth hole transport, HTLs reduce losses due to recombination, improving the internal quantum efficiency. Materials like PEDOT:PSS and Spiro-OMeTAD are commonly used for their superior processability, allowing for optimization of PSC performance. The HTL also plays a key role in optimizing the interface with the perovskite layer, by reducing defects and enhancing charge transport [32]. Spiro-OMeTAD is widely used due to its excellent hole mobility and energy level alignment, it suffers from limitations such as high material costs, complex doping requirements, and poor long-term stability under heat and moisture. Replacing Spiro-OMeTAD with inorganic Hole Transport Layers (HTLs) in perovskite solar cells (PSCs) offers several significant advantages in terms of stability. Furthermore, inorganic HTLs often exhibit lower production costs and simpler fabrication processes compared to Spiro-OMeTAD. Additionally, they can improve device efficiency by reducing charge recombination at the interface and providing better energy level alignment with the perovskite layer. Copper-based hole transporting materials have become prominent in perovskite solar cells due to their favorable characteristics, which contribute to enhanced device performance and scalability [33].

Specifically, materials such as copper iodide (CuI), copper thiocyanate (CuSCN), and cuprous oxide (Cu_2O) offer a cost-effective option compared to traditional organic HTMs like spiro-OMeTAD. These copper-based compounds exhibit superior hole mobility and conductivity, which are essential for efficient charge transport and reducing recombination losses in PSCs. Their fabrication is compatible with solution-based methods, facilitating scalable production. Moreover, the energy levels of these materials are optimally aligned with the perovskite layer, enabling efficient hole extraction and contributing to improved device efficiency. Nickel oxide (NiO) is also a promising material for hole transport layers (HTLs) in perovskite solar cells (PSCs), primarily due to its stability and versatility. Its environmental benignity and relatively low production costs render it an appealing choice for sustainable energy technologies. The electronic compatibility of NiO with perovskite materials facilitates efficient hole extraction and transport. Furthermore, the electronic properties of NiO can be tailored by modifying its composition, which enables the improvement the performance of PSCs.In this section, inorganic HTLs have been studied to replace the Spiro-OMeTad in the basic device. For this purpose, Cu_2O, CuI, CuSCN and NiO have been considered. the variation in power conversion efficiency as a function of the thickness of these HTLs is shown in Figure 3. The figure demonstrates a consistent trend across all structures with the different HTLs, where the conversion efficiency increases as a function of HTL layer thickness augmentation over the range of 100 nm to 500 nm. owever, The device incorporating the Cu_2O-HTL layer exhibited the highest efficiency, thereby identifying it as the optimal candidate. In accordance with the recommended guidelines for HTL layer thickness, an optimal thickness of 400 nm is selected.The photovoltaic parameters for the different HTL layers proposed have also been calculated and represented in Figure 4. Analysis of the results confirms what has already been seen in Figure 3, namely that the best performance is achieved by the Cu_2O-based structure.

3. 4 Impact of Interface Defect Density

The disparity in crystallographic structures between the electron transport layer (ETL), hole transport layer (HTL) and absorber layer can create numerous dislocations at their interfaces, degrading junction quality and increasing recombination losses. This effect is exacerbated by the misalignment of energy bands at these interfaces, which hampers charge transfer efficiency and promotes recombination. A key parameter reflecting these recombination processes is the surface recombination rate, which quantifies the speed at which charge carriers recombine at the interface, leading to performance degradation.In this context, the interface defect density was varied from 10^{10} cm^{-3} to 10^{20} cm^{-3} in order to assess its influence on device characteristics. Figure 5. illustrates how the interaction between defect density, band mismatch and recombination rate critically degrades the cell's electrical performance, highlighting the importance of minimizing interface defects and optimizing band alignment to improve solar cell efficiency.

3. 5 Optimization of the Back Metal Contact Layer

The optimisation of perovskite solar cells (PSCs) is strongly influenced by the work function of the metal contact [34]. This parameter plays a key role in aligning energy levels at the interface between the metal and the hole transport layer (HTL), thus affecting charge collection and overall device performance. High work function metals, such as platinum (Pt), are often preferred due to their ability to improve power conversion efficiencies (PCE) and open circuit voltages (Voc). Conversely, metals with a low work function, such as copper (Cu) and chromium (Cr), can compromise open-circuit voltage. In addition, the choice of metal contact has an impact on device stability and interfacial resistance. Conversely, metals with a low work function, such as copper (Cu) and chromium (Cr), can compromise open-circuit voltage. In addition, the choice of metal contact has an impact on device stability and interfacial resistance. While metals such as silver (Ag) and copper (Cu) show reduced stability and faster degradation, gold (Au) and platinum (Pt) offer superior stability at a higher cost. Specific metal contacts, including nickel (Ni), copper (Cu) and chromium (Cr), are compatible with spiro- OMeTAD, highlighting the importance of custom material selection to optimise PSC performance. Ultimately, careful consideration of the metal work function is crucial to improving the efficiency, stability and cost-effectiveness of perovskite solar cells. In this study several metals with defferent metal work funcion have been considered for back contact in the structure, the characteristics Current -Voltage of each one have been calculated and represented in Figure 6, and the corresonding photovoltaic performance and the rear energy barrier HTL/Metal height are shown in Table 4. When examining the current-voltage characteristics depicted in Figure 6 in addition to the results compiled in Table 4, it appears evident that the selection of metal for the back contact plays a crucial role in determining the performance of the

device. Notably, the open-circuit voltage is particularly sensitive to variations in the energy barrier Φ_b between the hole transport layer (HTL) and the back metal contact. This barrier's height is determined by two crucial factors: the valence band energy of the HTL material and the work function of the metal used for the back contact. As the work function of the metal augments from 4 eV to 5 eV, it is observed an obvious improvement in both the open-circuit voltage and the fill factor, which in turn enhances the overall power conversion efficiency of the solar cell.This is observed with Zinc, Silver, Chromium, and Carbon metal contacts. However, once the work function surpasses 5 eV, as seen with metal contacts like Gold and Platinum, the performance enhancements appear to reach a plateau, suggesting that further increases do not add additional benefits. These observations underscores the importance of carefully selecting the back contact metal to optimize solar cell performance. A back contact of carbon has been designed to replace the gold one in the optimized structure. The advantage of the latter is that it gives exactly the same performance as gold or platinum, as well as being cheaper than these noble metals.

3. 6 Impact of Parasitic Resistances R_s and R_{sh}

Parasitic resistances in perovskite solar cells are primarily categorized as series resistance (Rs) and shunt resistance (Rsh), both of which negatively influence device efficiency. The series resistance predominantly originates from the limited conductivity of the transparent conductive oxide (TCO) layer, typically around 10^{-4} Ω·cm for fluorine-doped tin oxide (FTO). Additionally, microstructural defects within the perovskite film, such as grain boundaries and voids, further impede charge carrier transport.Shunt resistance arises due to leakage currents caused by structural imperfections, including pinholes, cracks, or contaminants, which provide alternative pathways for current to bypass the active junction. Moreover, the formation of mixed interfacial layers at material interfaces—for example, between metal contacts and electron transport layers (ETLs), or between hole transport layers (HTLs) and TCOs—introduces additional electrical and optical parasitic losses. Together, these resistive elements contribute to a reduction in the fill factor and overall power conversion efficiency of perovskite solar cells. This section investigates the impact of varying parasitic resistances on the current-voltage (J-V) characteristics of the devices. The corresponding results are presented in Figure 6. The presence of a series resistor (R_s) reduces the slope of the current-voltage characteristic (J-V) shown in Figure 6 (a) in the vicinity of the maximum power point (MPP), thus lowering the fill factor (FF). However, R_s has a negligible influence on open-circuit voltage (V_{oc}) and induces only a marginal reduction in short-circuit current density (J_{sc}). Conversely, Figure 6 (b) confirms that the existence of a finite shunt resistance (R_{sh}) introduces leakage currents that reduce the colected current, leading to a drop in current density and overall power conversion efficiency (PCE). In addition, it was observed that shunt paths accelerate Voc degradation.These results underline the crucial importance of minimizing parasitic resistances - both series and shunt - in photovoltaic devices in order to maintain high performance and long-term stability.

4. Optimized Device and Performance

Taking into account the analysis of the results and all the previous observations, it was possible to design the following optimized structure: FTO/CeO_2/Cs_2PtI_6/Cu_2O/Carbon, with CeO_2-ETL, Cs_2PtI_6-absorber and Cu_2O-HTL layer thicknesses of 50nm, 2µm and 400µm and a carbon back metal contact. This structure is capable of increasing conversion efficiency to 18.54%.It is important to emphasize that the optimization work carried out in this project also contributes to the reduction of parasitic resistances by reducing recombination losses in the absorber mass, thanks to the control of manufacturing processes and also in the interfacial boundaries between layers by inter-layer passivation, in addition to the appropriate selection of ETL and HTL layer materials.Figure 7. compares the current-voltage curve of this structure with that of the primary structure. The results of the photovoltaic parameters are also compared with those of the primary structure in Table 5, as well as with those of some similar-material structures reported in the literature.As a consequence of the simulation and subsequent optimization process, the optimized solar cell structure showed improved performance, achieving a power conversion efficiency of 18.54%. In addition to the increased efficiency, it should be noted that the stability of the device was also improved, thanks to the adoption of an all-inorganic configuration through the selection of materials for the electron transport layer (ETL) and the hole transport layer (HTL). Furthermore, carbon was used as the back contact material, replacing the expensive gold contact used in the

basic structure. This substitution not only reduces the overall cost of the device, but also offsets the expense associated with the platinum-based noble metal incorporated in the perovskite active layer. Finally, compared with the performance of similar structures with close bandgap energies, it was observed that the results correlated well with devices based on lead-tin hybrid perovskite, as shown by the results reported in the references presented in Table 5. Compared with the performance of similar structures with close bandgap energies, it was observed that the results correlated well with devices based on lead-tin hybrid perovskite, as shown by the results reported in the references presented in Table 5.

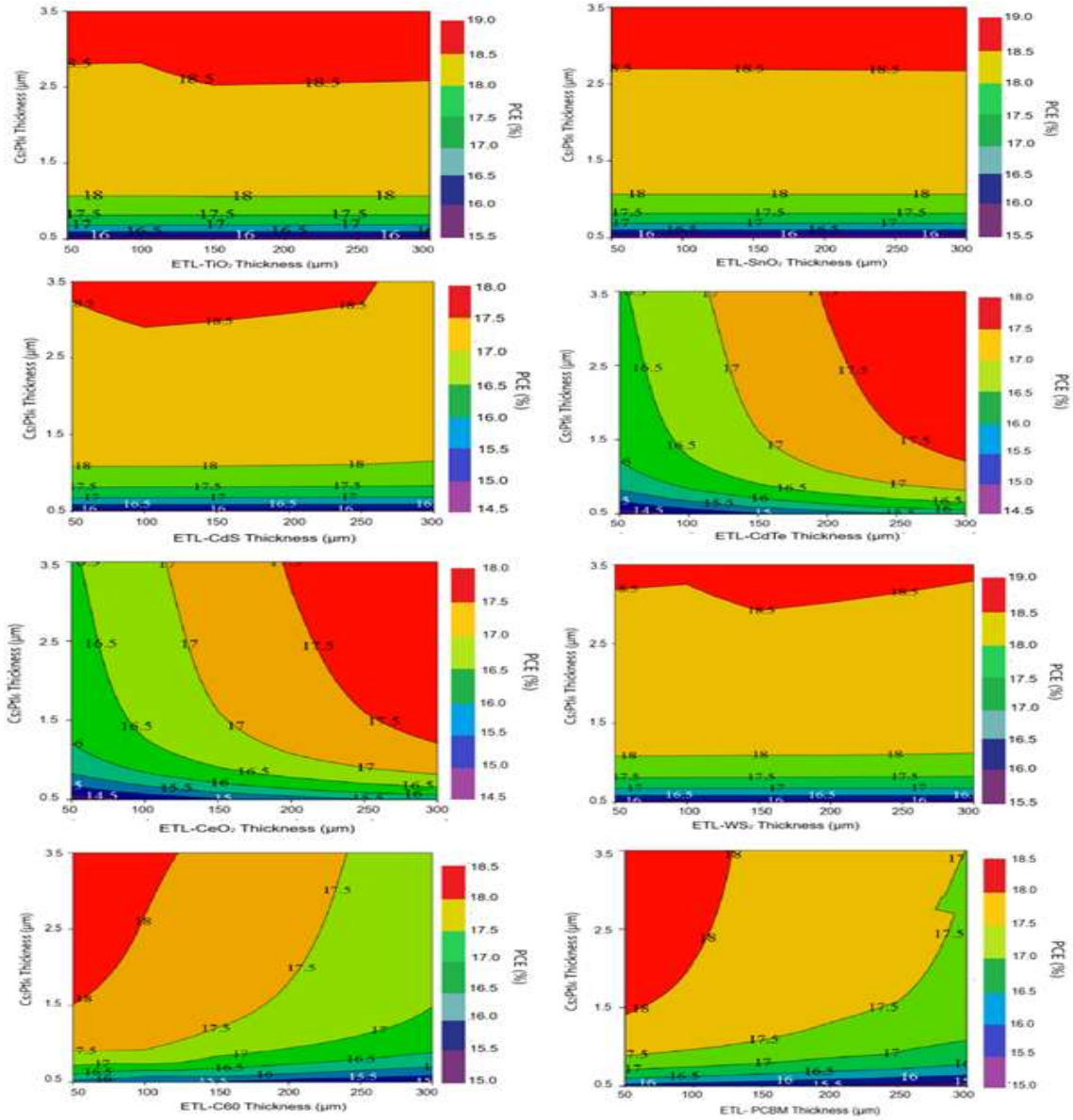

***Figure 2**. Power conversion efficiency (PCE) as a function of ETL and Cs_2PtI_6 thicknesses for various ETL. materials.*

***Table 3.** Power conversion Effiency of structures with Optimized thicknesses of ETL and Cs_2PtI_6*

Structure: ETL/Perovskite/HTL	**ETL Thickness (nm)**	**Cs_2PtI_6 Thickness (µm)**	**PCE (%)**
FTO/TiO_2/Cs_2PtI_6/Spiro-OMeTAD/Au	150	2.5	18.48
FTO/SnO_2/Cs_2PtI_6/Spiro-OMeTAD/Au	50	2.5	18.30
FTO/CdS/Cs_2PtI_6/Spiro-OMeTAD/Au	50	2.4	18.43
FTO/WS_2/Cs_2PtI_6/Spiro-OMeTAD/Au	150	2.5	18.45
FTO/CeO_2/Cs_2PtI_6/Spiro-OMeTAD/Au	50	2.0	18.48
FTO/CdTe/Cs_2PtI_6/Spiro-OMeTAD/Au	500	2.5	18.17
FTO/PCBM/Cs_2PtI_6/Spiro-OMeTAD/Au	50	2.0	18.15
FTO/C60/Cs_2PtI_6/Spiro-OMeTAD/Au	50	2.0	18.10

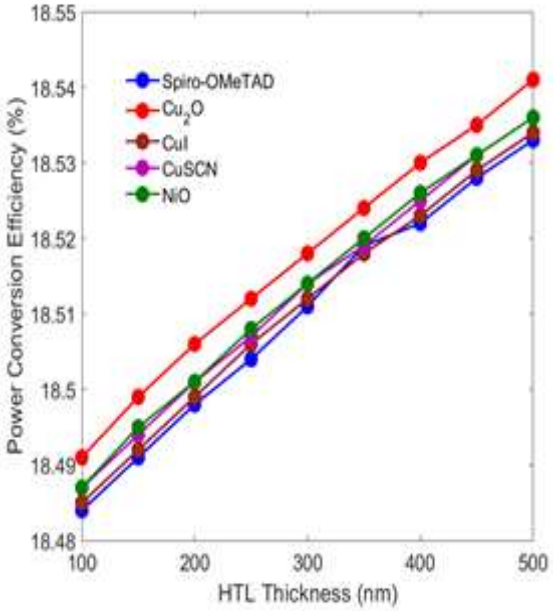

Figure 3. *Power conversion efficiency (PCE) as a function of HTL Thickness.*

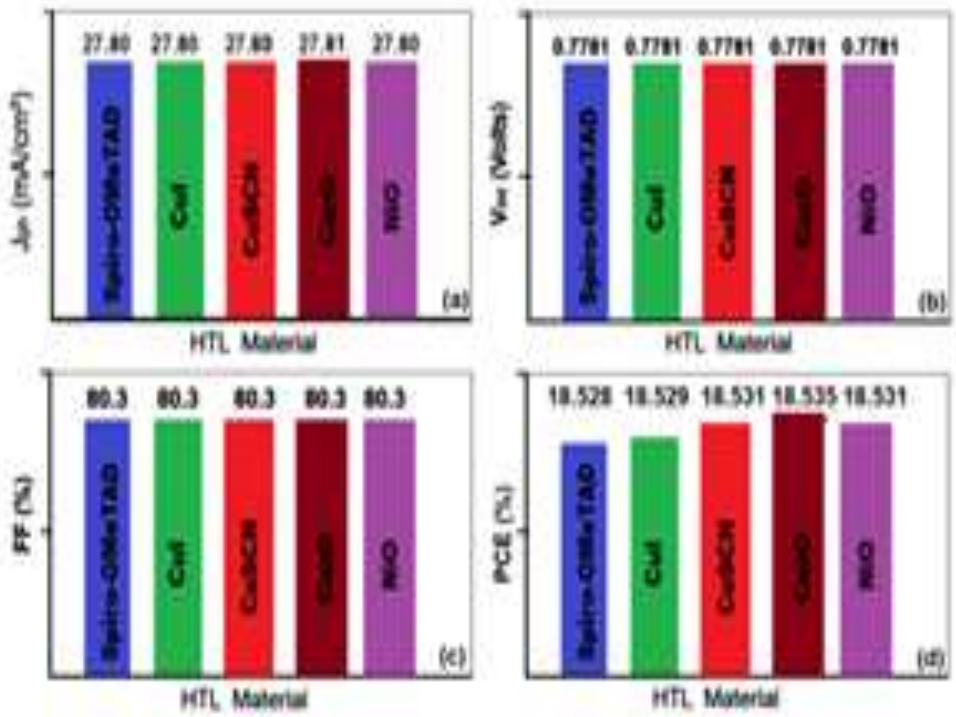

Figure 4. *Photovoltaic performance os structures based on HTLs Substitutes.*

Table 4 . *Impact of the Back Metal Contact on the Photovoltaic Performance of the Cs_2PtI_6 Cell*

Metal	**W_f (eV)**	**Φ_b (eV)**	**J_{ph} (mA/cm²)**	**V_{oc} (V)**	**FF (%)**	**PCE (%)**
Zinc	4.00	0.60	27.81	0.1342	25.50	1.02
Silver	4.40	1.00	27.81	0.7262	79.47	17.12
Chrome	4.50	1.10	27.81	0.7759	80.26	18.48
Carbon	5.00	1.60	27.81	0.7781	80.30	18.54
Gold	5.10	1.70	27.81	0.7781	80.30	18.54
Platinium	5.67	2.27	27.81	0.7781	80.30	18.54

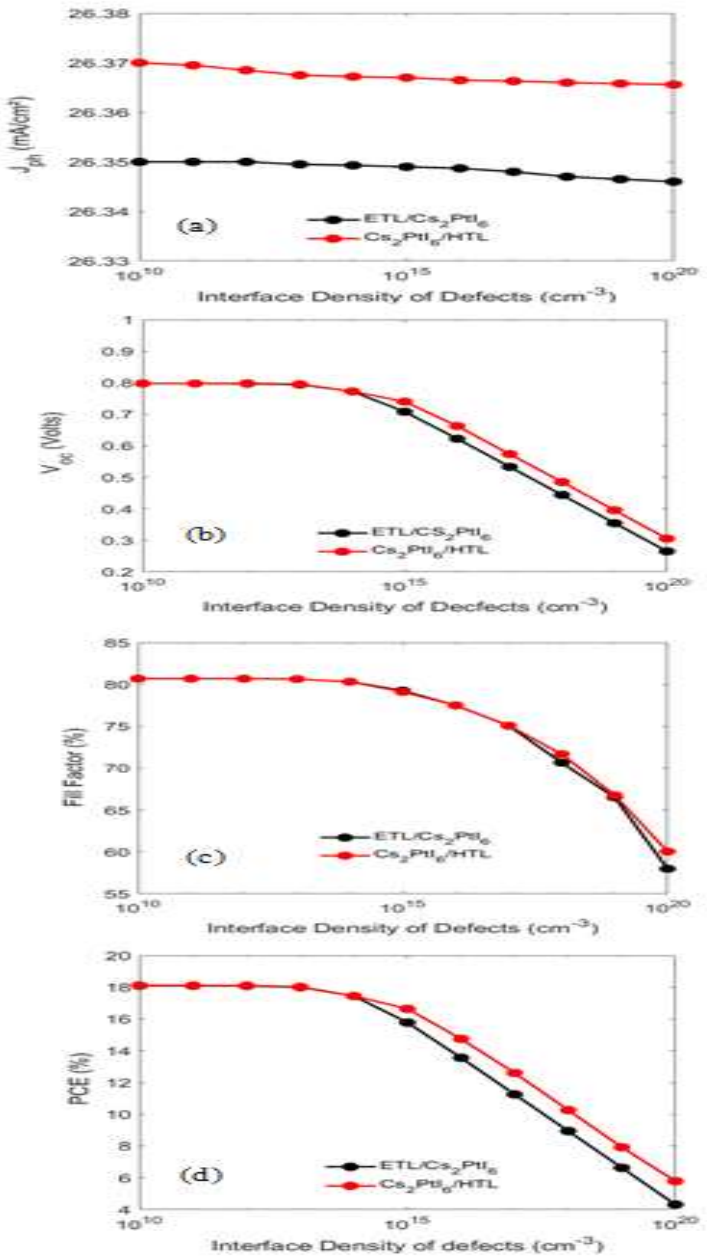

Figure 5. *Impact of Interface defect density on Key cell Parameteres*

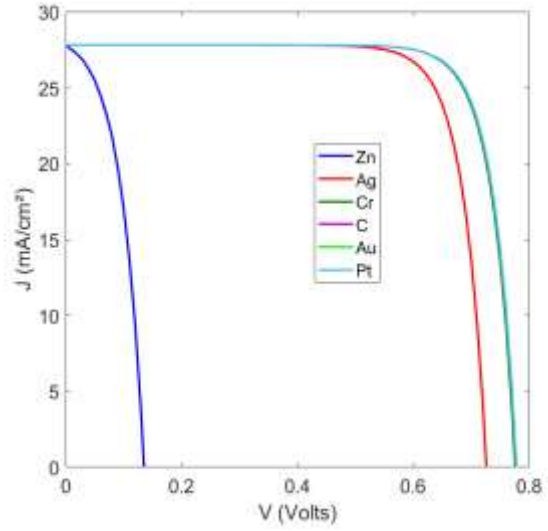

Figure 6*. Impact of The Back Metal Contact on the Current-Voltage Characteristics of the Optimized Structutre.*

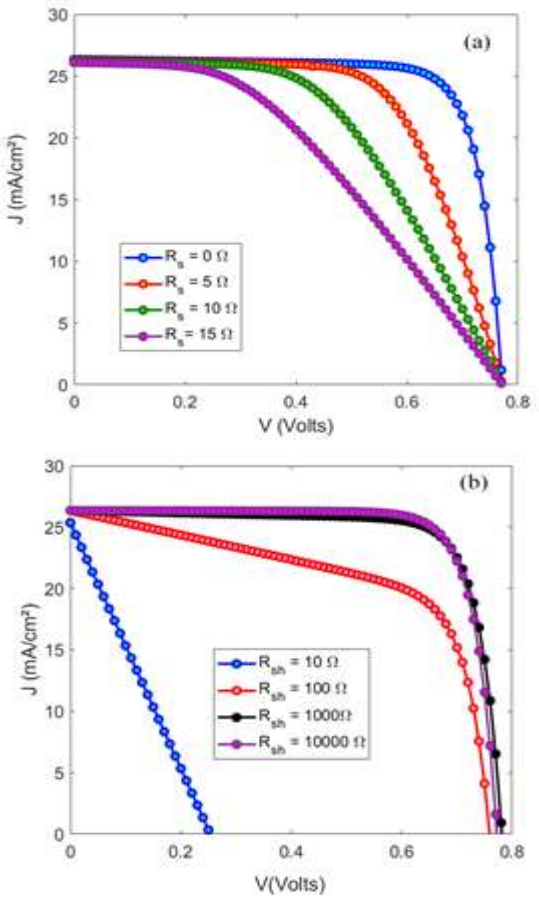

***Figure 6**. Impact of The Parasitic Resistances on J-V characteristics*

***Table 5** : Photovoltaic Performance Results and Comparison*

Structure	**Absorber**	**E_g (eV)**	**J_{ph} (mA/cm²)**	**V_{oc} (V)**	**FF (%)**	**PCE (%)**
Primary (This work)	Cs_2PtI_6	1.37	26.36	0.7731	80.34	17.46
Optimized (This work)	Cs_2PtI_6	1.37	27.81	0.7781	80.30	18.54
[35]	$MAPb_{0.9}Sn_{0.1}I_3$	1.40	23.39	0.9900	79.00	18.25
[36]	$CsPb_{0.6}Sn_{0.4}I_3$	1.38	24.57	0.7350	62.40	13.37
[37]	$MAPb_{0.85}Sn_{0.15}I_3$	1.34	30.37	0.8500	72.24	18.34

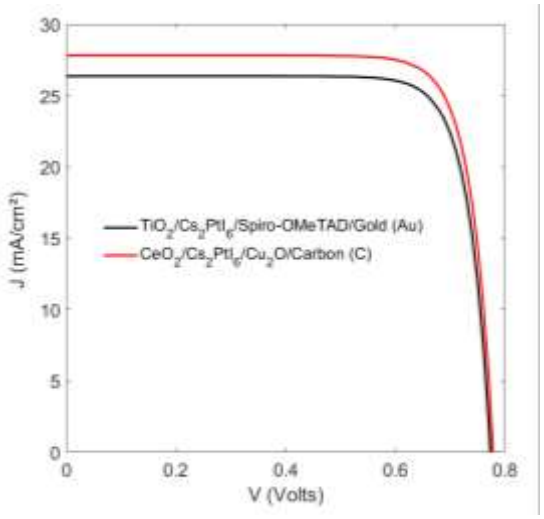

***Figure 7**. Comparison between Current-Voltage Curves of Optimized and primary Solar Cells.*

5. Conclusion

In this study, a solar cell structure based on the inorganic lead-free absorber Cs_2 PtI_6 was simulated and optimized. The developed simulation model enabled the calculation of the performance of the primary structure FTO/TiO_2 /Cs_2 PtI_6 /Spiro-OMeTAD/Gold and its dependence on key physical parameters and materials used for the different constituent layers. The results led to the determination of an enhanced structure that achieved a superior power conversion efficiency of 18.54% with a fully inorganic architecture and moderate use of noble elements, configured as FTO/CeO_2 /Cs_2 PtI_6 /Cu_2 O/Carbon. This simulation work is highly informative and could serve as a foundational theoretical study prior to the costly step of experimental realization. The aim is also to contribute to the advancement of high-efficiency, lead-free perovskite solar cells.

Author Statements:

- **Ethical approval:** The conducted research is not related to either human or animal use.
- **Conflict of interest:** The authors declare that they have no known competing financial interests or personal relationships that could have appeared to influence the work reported in this paper
- **Acknowledgement:** The authors declare that they have nobody or no-company to acknowledge.
- **Author contributions:** The authors declare that they have equal right on this paper.
- **Funding information:** The authors declare that there is no funding to be acknowledged.
- **Data availability statement:** The data that support the findings of this study are available on request from the corresponding author. The data are not publicly available due to privacy or ethical restrictions.

References

[1] Qusay Hassan, Sameer Algburi, Aws Zuhair Sameen, Tariq J. Al-Musawi, Ali Khudhair Al-Jiboory, Hayder M. Salman, Bashar Mahmood Ali, Marek Jaszczur,"A comprehensive review of international renewable energy growth,Energy and Built Environment",2024,ISSN 2666-1233, https://doi.org/10.1016/j.enbenv.2023.12.002.

[2] Mohsin Afroz, Ratneshwar Kumar Ratnesh, Swapnil Srivastava, Jay Singh, "Perovskite solar cells: Progress, challenges, and future avenues to clean energy", Solar Energy, Volume 287, 2025, 113205,ISSN 0038-092X, https://doi.org/10.1016/j.solener.2024.113205.

[3] Xiao Jia, Dan Yang, Dexu Zheng, Zhen Chang, Jishuang Liu, Lu Liu, Lei Peng, Yao Tong, Kai Wang, Shengzhong Liu," The progress and challenges of tin-lead alloyed perovskites: Toward the development of large-scale all-perovskite tandem solar cells ", Chem, Volume 11, Issue 1, 2025, 102384, ISSN 2451-9294, https://doi.org/10.1016/j.chempr.2024.12.002.

[4] D. Weber, "CH3NH3PbX3, ein Pb(II)-system mit kubischer perowskitstruktur/CH3NH3PbX3, a Pb(II)-system with cubic perovskite structure", Z. Naturforsch. B Chem. Sci. 33 (12) (Dec. 1978) 1443–1445

[5] Tayari, F.; Teixeira, S.S.; Graca, M.P.F.; Nassar, K.I. A Comprehensive Review of Recent Advances in Perovskite Materials: Electrical, Dielectric, and Magnetic Properties. *Inorganics* **2025**, *13*, 67. https://doi.org/10.3390/inorganics13030067

[6] Asir Eliet Magdalin, Peter Daniel Nixon, Elangovan Jayaseelan, Murugesan Sivakumar, Suresh Kumar Narmadha Devi, M.S.P. Subathra, Nallapaneni Manoj Kumar, Nallamuthu Ananthi,"Development of lead-free perovskite solar cells: Opportunities, challenges, and future technologies ", Results in Engineering, Volume 20, 2023, 101438, ISSN 2590-1230, https://doi.org/10.1016/j.rineng.2023.101438.

[7] Torrence CE, Libby CS, Nie W, Stein JS. Environmental and health risks of perovskite solar modules: Case for better test standards and risk mitigation solutions. iScience. 2022 Dec 15;26(1):105807. doi: 10.1016/j.isci.2022.105807. PMID: 36691614; PMCID: PMC9860350.

[8] Yang, C., Hu, W., Liu, J. *et al.* Achievements, challenges, and future prospects for industrialization of perovskite solar cells. *Light Sci Appl* **13**, 227 (2024). https://doi.org/10.1038/s41377-024-01461-x

[9] Aarif Ul Islam Shah, Edson Leroy Meyer, "Perovskite-based solar cells in photovoltaics for commercial scalability: Current progress, challenges, mitigations and future prospectus", Solar Energy, Volume 286, 2025, 113172, ISSN 0038-092X, https://doi.org/10.1016/j.solener.2024.113172.

[10] Arbouz, H. (2024). Investigation of Epitaxial Misfit Strain Influence at the CsSn(I1-xBrx)3/SnO2 Interface on Photovoltaic Parameters in Cu2O/CsSn(I1-xBrx)3/SnO2 Perovskite Solar Cells . International Journal of Computational and Experimental Science and Engineering, 10(4). https://doi.org/10.22399/ijcesen.367

[11] Arbouz, H. (2024). Optimization study of single junction structures utilizing 1.12 ev Cs2AuBiCl6 double perovskite: a lead-free inorganic absorber for single and tandem solar cell applications. Key Engineering Materials, 1003, 43-53. https://doi.org/10.4028/p-iiir9

[12]Ghorui, S., Kangsabanik, J., Aslam, M., & Alam, A. (2024). Optoelectronic and transport properties of vacancy-ordered double-perovskite halides: A first-principles study. Physical Review Applied, *21*(2), Article

024036. https://doi.org/10.1103/PhysRevApplied.21.024036

[13] Ruby Jindal, Archana Tripathi, Chandra Mohan, Alka Garg, Rajender S. Varma, "Lead-free halide double perovskites for sustainable environmental applications", Chemical Physics Impact, Volume 9, 2024, 100770, ISSN 2667-0224, https://doi.org/10.1016/j.chphi.2024.100770.

[14] Ye, Xinyu & Liu, Anmin & Gao, Liguo & Zhang, Chu & Lijing, Yan & Wen, Shizheng & Ma, Tingli. (2022). Computational screening of Cs based vacancy- ordered double perovskites for solar cell and photocatalysis applications. EcoMat. 5. 10.1002/eom2.12295.

[15] Zhao, Yinchang & Zeng, Shuming & Li, Geng & Lian, Chao & Dai, Zhenhong & Meng, Sheng & Ni, Jun. (2021). Lattice thermal conductivity including phonon frequency shifts and scattering rates induced by quartic anharmonicity in cubic oxide and fluoride perovskites. Physical Review B. 104. 224304. 10.1103/PhysRevB.104.224304.

[16] AbdElAziz HH, Taha M, El Rouby WMA, Khedr MH, Saad L. Evaluating the performance of Cs2PtI6-xBrx for photovoltaic and photocatalytic applications using first-principles study and SCAPS-1D simulation. Heliyon. 2022 Sep 28;8(10):e10808.doi:10.1016/j.heliyon.2022.e10808. PMID: 36203894; PMCID: PMC9530494.

[17] Schwartz, Dakota & Murshed, Rubaiya & Larson, Harry & Usprung, Benedikt & Soltanmohamad, Sina & Pandey, Ramesh & Barnard, Edward & Rockett, Angus & Hartmann, Thomas & Castelli, Ivano & Bansal, Shubhra. (2020). Air Stable, High Efficiency, Pt-Based Halide Perovskite Solar Cells with Long Carrier Lifetimes. physica status solidi (RRL) - Rapid Research Letters. 14. 10.1002/pssr.202000182.

[18] Diwen Liu, Caihua Zhang, Rongjian Sa,The fundamental physical properties of Cs2PtI6 and (CH3NH3)2PtI6,Physica B: Condensed Matter, Volume 644, 2022, 414235, https://doi.org/10.1016/j.physb.2022.414235.

[19] Amjad A, Qamar S, Zhao C, Fatima K, Sultan M, Akhter Z. Numerical simulation of lead-free vacancy ordered Cs2PtI6 based perovskite solar cell using SCAPS-1D. RSC Adv. 2023 Aug 1;13(33):23211-23222. doi: 10.1039/d3ra04176j. PMID: 37533780; PMCID: PMC10392039.

[20] Faizan, M., Bhamu, K.C., Murtaza, G. *et al.* Electronic and optical properties of vacancy ordered double perovskites A2BX6 (A = Rb, Cs; B = Sn, Pd, Pt; and X = Cl, Br, I): a first principles study. *Sci Rep* **11**, 6965 (2021). https://doi.org/10.1038/s41598-021-86145-x

[21] Murugan, S.; Lee, E.-C. Recent Advances in the Synthesis and Application of Vacancy-Ordered Halide Double Perovskite Materials for Solar Cells: A Promising Alternative to Lead-Based Perovskites. Materials 2023, 16, 5275. https://doi.org/10.3390/ma16155275

[22] Rehman, U.u., Almousa, N., Sahar, K.u., Ashfaq, A., Mahmood, K., Shokralla, E.A., Al-Buriahi, M.S., Alrowaili, Z.A., Capangpangan, R.Y. and Alguno, A.C. (2023), Optimizing the Efficiency of Lead-Free Cs2TiI6-Based Double Halide Perovskite Solar Cells Using SCAPS-1D. Energy Technol., 11: 2300459. https://doi.org/10.1002/ente.202300459

[23] Moiz, S. A., Alahmadi, A. N. M., & Aljohani, A. J. (2021). Design of a Novel Lead-Free Perovskite Solar Cell for 17.83% Efficiency. IEEE Access, 9, 54254–54263. doi:10.1109/access.2021.3070112

[24] M. Khalid Hossain, Apon Kumar Datta, Osamah Alsalman, M. Shihab Uddin, Gazi F.I. Toki, Moustafa A. Darwish, M.R. Mohammad, D.K. Dwivedi, Rajesh Haldhar, Sergei V. Trukhanov,"An extensive study on charge transport layers to design and optimization of high-efficiency lead-free Cs2PtI6-based double-perovskite solar cells: A numerical simulation approach", Results in Physics, Volume 61, 2024, 107751,ISSN 2211-3797, https://doi.org/10.1016/j.rinp.2024.107751.

[25] S. T. Jayawardane, M. D. Akmal, Y. H. Jayaneththi, T. V. Fernando, D. Hu, P. K. W. Abeygunawardhana, G. A. Sewvandi, Simulation-Based Performance Analysis of Lead-Free Bismuth Perovskite Solar Cells: A Comparative Study of Cs3Bi2I9 and (CH3NH3)3Bi2I9 -based Perovskite Solar Cells. *Adv. Theory Simul.* 2024, 7, 2400206. https://doi.org/10.1002/adts.202400206

[26] Shivesh K, Alam I, Kushwaha AK, Kumar M, Singh SV. Investigating the theoretical performance of Cs2TiBr6-based perovskite solar cell with La-doped BaSnO3 and CuSbS2 as the charge transport layers. *Int J Energy Res*. 2022; 46(5): 6045-6064. https://doi.org/10.1002/er.7546

[27] Aliani, C., Krichen, M. & Zouari, A. Effect of the front-metal work function on the performance of a-Si:H(n^+)/a-Si:H(i)/c-Si(p) heterojunction solar cells. *J Comput Electron* **18**, 576–583 (2019). https://doi.org/10.1007/s10825-019-01324-4

[28] M. Courel, J. A. Andrade-Arvizu, O. Vigil-Galán, "The role of buffer/kesterite interface recombination and minority carrier lifetime on kesterite thin film solar cells," Mater. Res. Express, vol. 3. 9, 2013, 095501. DOI 10.1088/2053-1591/3/9/095501

[29] Md. Ariful Islam Bhuiyan, Md. Shamim Reza, Avijit Ghosh, Hmoud Al-Dmour, Yedluri Anil Kumar, Muhammad Ihsan Ibn Rahim, Md. Aktarujjaman, Fahima Yeasmin, Hamad Al-Lohedan, R. Jothi Ramalingam, Md. Selim Reza,"Optimized RbPbI3-Based perovskite solar cells with SnS2 ETL and MoO3 HTL achieving simulated PCE of 32.72%," Optics Communications, Volume 583, 2025, 131761, ISSN 0030-4018, https://doi.org/10.1016/j.optcom.2025.131761.

[30] Z. Guo, M. Yuan, G. Chen, F. Liu, R. Lu, W.-J. Yin, Understanding Defects in Perovskite Solar Cells through Computation: Current Knowledge and Future Challenge. *Adv. Sci.* 2024, 11, 2305799. https://doi.org/10.1002/advs.202305799.

[31] Gamal, K., Gamal, M., Okaz, A. et al. Comprehensive performance analysis of perovskite solar cells based on different crystalline

structures of MAPbI3. Opt Quant Electron 56, 827 (2024). https://doi.org/10.1007/s11082-024-06655-6

[32] Y. Yao, C. Cheng, C. Zhang, H. Hu, K. Wang, S. De Wolf, Organic Hole-Transport Layers for Efficient, Stable, and Scalable Inverted Perovskite Solar Cells. *Adv. Mater*. 2022, 34, 2203794. https://doi.org/10.1002/adma.202203794

[33] Jadel Tsiba Matondo, Davy Malouangou Maurice, Qin Chen, Luyun Bai, Mina Guli, "Inorganic copper-based hole transport materials for perovskite photovoltaics: Challenges in normally structured cells, advances in photovoltaic performance and device stability," Solar Energy Materials and Solar Cells, Volume 224, 2021, 111011, ISSN 0927-0248, https://doi.org/10.1016/j.solmat.2021.111011.

[34] Fan Zhang, Wenjing Hou, Helin Wang, Jun Song, "Improving the performance and stability of inverted perovskite solar cell modules by cathode interface engineering," Chemical Engineering Journal, Volume 490, 2024, 151805, ISSN 1385-8947, https://doi.org/10.1016/j.cej.2024.151805.

[35] Yin, Y., Fu, S., Zhou, S. *et al.* Efficient and Stable Ideal Bandgap Perovskite Solar Cell Achieved by a Small Amount of Tin Substituted Methylammonium Lead Iodide. *Electron. Mater. Lett.* **16**, 224–230 (2020). https://doi.org/10.1007/s13391-020-00206-3

[36] Hu, M., Chen, M., Guo, P. et al. Sub-1.4eV bandgap inorganic perovskite solar cells with long-term stability. Nat Commun 11, 151 (2020). https://doi.org/10.1038/s41467-019-13908-6

[37] Wenxiao Zhang, Xiaodong Li, Sheng Fu, Xiaoyan Zhao, Xiuxiu Feng, Junfeng Fang," Lead-lean and MA-free perovskite solar cells with an efficiency over 20%," Joule, Volume 5, Issue 11, 2021, Pages 2904-2914, ISSN 2542-4351, https://doi.org/10.1016/j.joule.2021.09.008.